Title: **Activity-dependent long-term potentiation of electrical synapses in the mammalian thalamus**

Running title: LTP of electrical synapses

Summary: Long-term potentiation results from spiking in one cell of an electrically coupled pair. Asymmetry of synapses increases following unidirectional activity. We suggest a calcium-based rule for electrical synapse plasticity.

Authors: Brandon Fricker[1], Emily Heckman[1,2], Patrick C. Cunningham[1], and Julie S. Haas[1,*]

Affiliations: 1. Department of Biological Sciences, Lehigh University
111 Research Drive
Bethlehem, PA 18015
2. Present address: Institute of Neuroscience, Department of Biology, University of Oregon,
1254 University of Oregon,
Eugene, OR 97403
*to whom correspondence should be addressed: julie.haas@lehigh.edu

Keywords: activity dependent plasticity, electrical synapse, gap junction, LTP, asymmetry

Acknowledgements: Bruce Bean (Harvard) generously supplied TTA-A2. We thank C. E. Landisman, R. M. Burger, T. Pham and all Haas lab members for input on drafts of this manuscript. Funding was provided by the NSF (IOS 1557474), the Whitehall Foundation, and the Brain & Behavior Foundation.

Abstract

Activity-dependent changes of synapse strength have been extensively characterized at chemical synapses, but the relationship between physiological forms of activity and strength at electrical synapses remains poorly understood. For mammalian electrical synapses composed of hexomers of connexin36, physiological forms of neuronal activity in coupled pairs has thus far have only been linked to long-term depression; activity that results in strengthening of electrical synapses has not yet been identified. The thalamic reticular nucleus (TRN), a central brain area primarily connected by gap junctional (electrical) synapses, regulates cortical attention to the sensory surround. Bidirectional plasticity of electrical synapses may be a key mechanism underlying these processes in both healthy and diseased states. Here we show in electrically coupled TRN pairs that tonic spiking in one neuron results in long-term potentiation of electrical synapses between coupled pairs of TRN neurons. Potentiation is expressed asymmetrically, indicating that regulation of connectivity depends on the direction of use. Further, potentiation depends on calcium flux, and we thus propose a calcium-based activity rule for bidirectional plasticity of electrical synapse strength. Because electrical synapses dominate intra-TRN connectivity, these synapses and their modifications are key regulators of thalamic attention circuitry. More broadly, bidirectional modifications of electrical synapses are likely to be a widespread and powerful principle for ongoing, dynamic reorganization of neuronal circuitry across the brain.

Introduction

The thalamic reticular nucleus (TRN) is a central brain region exclusively comprising inhibitory neurons that gate the bidirectional flow of information between thalamus and cortex, and ultimately regulate the cognitive process of attention (Halassa et al., 2014; Kimura, 2014; McAlonan et al., 2006; Sherman, 2016; Zikopoulos & Barbas, 2012). Like all thalamic neurons, TRN neurons fire action potentials in two modes (Contreras et al., 1992). Bursts, which feature a slow calcium spike from a T-type calcium current (Huguenard & Prince, 1992) crowned by a fast barrage of sodium spikes, dominate TRN activity during slow sleep rhythms (Crunelli et al., 2006; Destexhe et al., 1996; Huguenard & Prince, 1992; McCormick & Bal, 1997; Steriade et al., 1993), are a feature of *absence* epilepsy (Fuentealba & Steriade, 2005), and are reduced in schizophrenics (Ferrarelli & Tononi, 2011). Regular tonic spikes, in contrast, are prevalent during attentive behaviors (Pinault, 2004). Because the main mode of intra-TRN communication is its dense electrical synapses (Hou et al., 2016; Landisman et al., 2002), understanding how and when electrical synapses change in strength during these two modes of activity is key for understanding attention processes and rhythm generation.

In the mature mammalian brain, electrical synapses are composed of paired hexomers of connexin36 that pass ions and small molecules, and mainly couple inhibitory GABAergic neurons (Bennett & Zukin, 2004; Connors & Long, 2004; Galarreta & Hestrin, 2001). Electrical synapses contribute to synchrony in coupled networks (Chow & Kopell, 2000; Destexhe, 1998; Draguhn et al., 1998; Gutierrez et al., 2013; Haas & Landisman, 2012; Pernelle et al., 2018; Pfeuty et al., 2005; Wang & Rinzel, 1993; Whittington & Traub, 2003) and regulate timing of spikes in the neurons they couple (Haas, 2015; Pham & Haas, 2018, 2019). Despite their prevalence and function between spiking neurons across the brain, the effects of neuronal activity on connection strength remain sparsely characterized. A line of work in non-mammalian nervous systems has demonstrated the possibility for central electrical synapses to undergo

plasticity (McMahon et al., 1989; Pereda & Faber, 1996; Welzel & Schuster, 2018; Yang et al., 1990). In the mammalian brain, synaptic input has been shown to modulate mammalian electrical synapses in the inferior olive (Lefler et al., 2014) in an NMDA-dependent manner (Mathy et al., 2014; Turecek et al., 2014), and tetanic glutamatergic input to coupled TRN neurons results in long-term depression (LTD)(Landisman & Connors, 2005). The impact of spiking in coupled neurons on electrical synapses is much less well understood. We previously showed that LTD of electrical synapses in TRN also follows bursting activity of coupled neurons (Haas et al., 2011) in a calcium-dependent manner (Sevetson et al., 2017), but a link between activity in coupled neurons and strengthening of the synapse has remained elusive.

Here we demonstrate, using dual whole-cell patch recordings, that long-term potentiation (LTP) of electrical synapses in the TRN follows low-frequency spiking in one of the cells. LTP is specific to single-cell activity, and depends on calcium influx. We show that the increase in coupling strength is expressed in an asymmetrical manner that depends on the direction of synapse use. Combined with results of calcium imaging during activity, our work leads us to propose a calcium-based activity dependent plasticity rule for electrical synapses.

Results

Thalamic neurons fire action potentials (APs) in two modes: from hyperpolarized resting potentials, bursts of calcium spikes crowned by a quick sequence of sodium spikes; and from depolarized rests, regular (tonic) sodium spikes (Fig. 1A). Having previously established that bursting in coupled TRN neurons leads to long-term depression of the electrical synapse between them (Haas et al., 2011) as a result of large-conductance, T-channel mediated calcium influx during bursts (Sevetson et al., 2017), we reasoned that tonic spikes and smaller calcium influx might lead to potentiation of electrical synapse strength. In order to minimize activation of the low voltage-activated T-type calcium current that underlies bursts, we added the specific antagonist TTA-A2 (Kraus et al., 2010) (1 μM) to the ACSF bath solution. We applied steady

current to raise the membrane potential of one cell of a coupled pair at or above -55 mV, again to minimize the T current, while maintaining its coupled neighbor at -70 mV. We measured electrical coupling in each direction separately (Fig. 1B). We then applied small-amplitude, long pulses of current to the depolarized cell to induce non-continuous tonic spiking for 5 minutes, resulting in a spiking frequency of 5 - 10 Hz (Fig. 1C). After 5 minutes of tonic spiking activity in one neuron, coupling conductance measured from the quiet cell into the active cell increased on average by 15.5% ± 2.3% (p_t = 0.004) and coupling coefficient in the same direction increased by 13.6 ± 2.2% (Fig. 1E–F; p_t = 0.01, n = 12 pairs). Coupling measured by current injection into the active cell, in contrast, did not change in conductance (-1.5 ± 0.5%, p_t = 0.78) while coefficients in this direction decreased by 7.6 ± 0.5% (p_t = 0.018). Input resistance in the quiet cell decreased by 5.5 ± 0.4% (Fig. 1G; p_t = 0.0005), while input resistance in the active cell was unchanged (p_t = 0.73; sign tests performed on changes in cc and Gc gave similar results). Input resistance and coupling coefficients are directly related; thus it is difficult to determine whether the decrease in R_{in} caused the apparent decrease in cc or *vice versa*, but this dependence is minimized by the calculation of G_C, which demonstrated clear changes in only one direction in this experiment. LTP was sustained for more than 25 minutes after induction.

LTP was specific to single-cell stimulation: paired activity in TTA did not significantly change synapse strength (Fig. 2A; p_t > 0.05 for both changes in cc and G_C, averaged over both directions for paired activity, n = 8 pairs), and paired tonic spiking in unmodified ACSF also failed to change synapse strength (Fig. 2B; p_t > 0.05 for both changes in cc and G_C, n = 6 pairs).

We hypothesized that the LTP we observed might be dependent on the smaller amounts of calcium influx from high-voltage activated channels (Budde et al., 1998). When we repeated single-cell tonic spiking in TTA with BAPTA in the pipettes to rapidly chelate all influxed calcium within both neurons, we observed no LTP (Fig. 2C; p_t > 0.05 for both directions of changes in cc or G_C, n = 7 pairs). Single-cell spiking in unmodified ACSF also failed to induce changes in

synaptic strength (Fig. 2D; $p_t > 0.05$ for both directions of changes in cc or G_C, n = 9 pairs). Together, these results outline a calcium dependence of plasticity: minimal influx of calcium during single-cell tonic spiking, possibly buffered by the quiet cell, leads to LTP, while larger influx of calcium during paired tonic spiking activity exceeds that required for LTP, instead activating the mechanisms leading to LTD (Sevetson et al., 2017).

Our hypothesis that the LTP we saw arose from the minimal amount of calcium influx revealed by TTA and depolarization of the active cell led us to further investigate differences in calcium influx and transmission across the gap junction during the two different modes of induced activity. We therefore performed imaging experiments of pairs with the calcium indicator OGB-1 included in the internal solution (Fig. $3A_1$). We drove one cell to spike either in bursts or in tonic mode, while we held the quiet cell in held in voltage-clamp mode at -70 mV to minimize calcium signals arising from voltage-activated channels. During the induced bursting in one cell that leads to LTD (Haas et al., 2011), both peak and integrated calcium levels were higher in the active cell and in the quiet coupled neighbor than during induced tonic spiking (Fig. $3A_2$-A_4). As a negative control, we repeated the imaging in a non-coupled pair (Fig. $3B_{1\text{-}4}$). Quantification of peak and integrated calcium signals in the quiet, coupled cells (Fig. 3C, D) both indicate that less calcium flows across the gap junction during tonic spiking than during bursting (for AUC, -25.2 ± 10.6%, $p_s = 0.06$; for peak calcium, -56.6 ± 10.9%, $p_s = 0.03$, n = 6 pairs).

The LTP we observed that resulted from single-cell activity was expressed asymmetrically: coupling into the active cell increased, while coupling into the quiet cell decreased (Fig. 1). To examine whether this asymmetrical plasticity was consistent across pairs, we computed asymmetry as the ratio of coupling measured into the active cell, divided by coupling measured from the active cell. Those ratios consistently increased after LTP induction for both coupling coefficient (Fig. 4A; mean increase 24.3 ± 6.2%, $p_t = 0.0015$, $p_s = 0.008$, n = 12 pairs) and conductance (Fig. 4B: mean increase 22.4 ± 8.2%, $p_t = 0.029$, $p_s = 0.008$). We

noted that some pairs went from initially symmetrical, to finally asymmetric, and *vice versa*. Changes in coupling asymmetry were uncorrelated with changes in R_{in} ratios (R^2 = 0.39 for cc and 0.03 for G_C). These results are consistent with the asymmetrical changes we also observed for burst-induced LTD (Haas et al., 2011) in that both asymmetrical LTP and LTD required sodium spikes, and changes were larger for coupling measured into the active cell. These changes in asymmetry indicate that the unidirectional use of the electrical synapse, and perhaps unidirectional calcium flow, systematically alter the fundamental property of each synapse.

Together, our results lead us to propose a calcium rule for plasticity of electrical synapses, whereby smaller amounts of calcium influx lead to LTP, and larger amounts lead to LTD (Fig. 5). The proposed rule is similar in concept to those proposed (Bienenstock et al., 1982; J. Lisman, 1989) (J. E. Lisman, 2001)and demonstrated (Dudek & Bear, 1992; Malenka & Bear, 2004; Malenka et al., 1989) at glutamatergic synapses.

Discussion

Here we show that long-term potentiation of electrical synapses results from tonic spiking in a single cell of the electrically coupled pair. To our knowledge, this is the first demonstration of LTP in mammalian electrical synapses that results from spiking activity within coupled neurons and flow of ions across the synapse. Moreover, our results taken together indicate a bidirectional calcium dependence of activity-dependent plasticity at electrical synapses, whereby high calcium influx and flow across the gap junction leads to LTD (Haas et al., 2011; Sevetson et al., 2017) while minimal calcium influx and flow across the gap junction leads to LTP. The links established here between physiological patterns of spiking activity in TRN neurons demonstrate that ongoing plasticity of electrical synapses is likely to occur in the active brain. As calcium rules are common for chemical synapses, we expect that calcium dependent rules, possibly in different forms, will underlie plasticity of electrical synapses across the brain.

The magnitude of LTP-induced changes in electrical synapse strength are similar in magnitude to our previous demonstration of LTD, less than 20% (GC or cc). These are modest changes relative to those often demonstrated at chemical synapses driven by tetanic stimulation. A direct comparison between synapse types and plasticity would need to account for differences in subcellular localization differences and differences in function, for instance spike efficacy. However, for LTD we showed that these changes were sufficient to silence a synapse, from one that induces spikes in neighbors, to an ineffective synapse (Haas et al., 2011). Further, these numerically modest changes in synaptic strength yield 5-10 ms changes in spike times in coupled neighbors (Haas, 2015). Computational models reinforce the effectiveness of changes in coupling in this range (Pham & Haas, 2018, 2019). Thus, even seemingly modest changes in electrical synapse strength produce physiologically substantial effects, and are poised to exert major influence on TRN synchrony and processing.

Our experiments required minimization of T currents by TTA in order to reveal conditions favorable for LTP at electrical synapses. While this is not strictly a physiological condition, we expect that together with depolarization of the active cell, these perturbations were necessary to counterbalance the artificial quiescence and hyperpolarization of the brain slice preparation, in which almost any depolarization of thalamic neurons activates T currents and thereby LTD. We expect that LTP is more likely to occur in vivo during prolonged depolarizations when tonic spiking dominates spiking patterns (Pinault, 2004). We further hypothesize that during tonic spiking in one neuron, calcium influx into the active cell is buffered across the gap junction by the quiet cell (Fig. 2, 3). Together, these results imply that LTP can be initiated by tonic spikes in single neurons, and subsequently counterbalanced by LTD resulting from bursts; together, these form a bidirectional basis for active neurons to modify the gain of their inputs.

Although functional asymmetry is not an expected property of gap junctions purely composed of connexin36 hemichannels (Srinivas et al., 1999), it has been observed as a

widespread property of mammalian electrical synapses (Apostolides & Trussell, 2014; Devor & Yarom, 2002; Otsuka & Kawaguchi, 2013; Sevetson & Haas, 2015; Snipas et al., 2017; Vervaeke et al., 2010; Zolnik & Connors, 2016). Our previous results demonstrated that asymmetry systematically increases during LTD induced by asymmetrical bursting activity (Haas et al., 2011). Asymmetry was also shown to increase following LTP produced by NMDA application (Turecek et al., 2014) or by cerebellar input to coupled inferior olivary neurons (Lefler et al., 2014). Our results here add further evidence towards modifications of asymmetry that occur during plasticity; both our previous LTD results and the present LTP results indicate that sodium spikes are necessary for changes in asymmetry, and that changes are larger in the direction incoming to the active neuron. Together, these reports form a growing consensus that asymmetry and asymmetrical changes are a fundamental property of electrical synapses that potentially refine the function of each individual synapse within its neuronal circuit, allowing for each neuron to adjust the relative proportion of input it sends and/or receive from coupled neighbors via electrical synapses. Differences in intracellular scaffolding proteins have been shown to construct asymmetrical electrical synapses in zebrafish (Marsh et al., 2017). We suggest that increased expression or open probability of more-asymmetrical non-connexin36 proteins (Zolnik & Connors, 2016) could also account for this activity-dependent increase in asymmetry. Alternatively, differential post-translational modification, such as asymmetrical phosphorylation of cx36 hemichannels, or differences in ubiquitination-mediated endocytosis (Lynn et al., 2018), or the hypothesized effects of gating properties of the channel (Snipas et al., 2017) remain possible. In TRN, calcium bursts are activated in dendrites independently of somatic compartments, which could further result in independent modifications of one side of the gap junction. Asymmetry can strongly influence spike times in coupled pairs (Sevetson & Haas, 2015) and thereby impact cortical discrimination through the thalamocortical circuit (Pham & Haas, 2018). We suggest that it may also take part in directional signaling mediated by

197 electrical synapses, such as that found in direction-sensitive retinal ganglion cells (Yao et al.,
198 2018).

199 Based on our previous and current work, we propose a calcium rule for bidirectional
200 activity-dependent plasticity at electrical synapses. This rule is 'inverse' to those described for
201 chemical synapses, where smaller calcium influx produces LTD while larger influxes lead to LTP
202 (Bienenstock et al., 1982; Dudek & Bear, 1992; Malenka et al., 1989). Notably, an inverse rule
203 for chemical synapses also exists in the cerebellum (Coesmans et al., 2004). As previous
204 studies have found that LTD is induced by calcium-based pathways leading to phosphatase
205 activation (Sevetson et al., 2017), we expect that LTP may depend on a phosphorylation
206 mechanism initiated by calcium. Retinal coupling depends on phosphorylation (Kothmann et al.,
207 2007), and tetanus-induced forms of plasticity at mixed synapses onto Mauthner cells in goldfish
208 depend on NMDA-regulated calcium entry (Pereda & Faber, 1996; Yang et al., 1990). Recent
209 work has also shown that spiking-initiated calcium entry leads to potentiation for up to 10 min. at
210 an invertebrate electrical synapse (Welzel & Schuster, 2018). While not directly examined, our
211 results imply that the threshold between the concentration of calcium for LTP and LTD is rather
212 low, as even paired tonic spiking fails to induce LTP, and the T current that underlies burst-
213 induced LTD is active at rest potentials. This bias of plasticity towards LTD, however, could be
214 specific to brain-slice conditions, as addressed above. We find it likely that electrical synapses
215 across the brain follow a calcium-based rule for plasticity, although non-bursting neuronal types
216 may alternatively follow a different rule.

217 A role for plasticity of electrical synapses has been proposed for switches in attentional
218 state (Coulon & Landisman, 2017). Taken together, our results demonstrate that the strength of
219 electrical synapses can be modified positively or negatively in strength as a result of
220 physiological activity in the TRN, and with neuron-specific directionality. For single cells, activity-
221 dependent plasticity of electrical synapses could modulate that cell's input sensitivity between

modes in which intra-TRN input is strongest and dominates its responses, to modes in which corticothalamic or thalamocortical chemical input is given preference over electrically networked signals. This high degree of acuity and adjustability of connectivity within coupled networks forms a basis for shifts of sensory attention regulated by the TRN. TRN neurons can toggle thalamic neurons between firing modes in order to maintain cortical sleep rhythms and the associated behaviors of that state (Sorokin et al., 2017), and the activity and synchrony of TRN neurons required for that toggle may be supplied by its electrical synapses. Sensory processing of selective features (Soto-Sanchez et al., 2017) is also likely to depend on acutely refined TRN connectivity in a similar manner. Beyond the TRN and its functions, our work shows that electrically coupled networks are potentially under a high degree of regulation of function throughout the mammalian brain.

Methods

Electrophysiology

All experiments were performed in accordance with federal and Lehigh University IACUC animal welfare guidelines. Sprague-Dawley rats of both sexes aged postnatal day 11-15 were anesthetized by inhaled isoflurane (5 mL of isoflurane applied to fabric, within a 1 L chamber) and sacrificed via decapitation. Horizontal brain slices 300-400 µm thick were cut and incubated in sucrose solution (in mM): 72 sucrose, 83 NaCl, 2.5KCl, 1 $NaPO_4$, 3.3 $MgSO_4$, 26.2 $NaHCO_3$, 22 dextrose, 0.5 $CaCl_2$. Slices were incubated at 37°C for 20 min following cutting and returned to room temperature until recording. The bath for solution during recording contained (in mM): 126 NaCl, 3 KCl, 1.25 NaH_2PO_4, 2 $MgSO_4$, 26 $NaHCO_3$, 10 dextrose and 2 $CaCl_2$, 300–305 mOsm L^{-1}, saturated with 95% O_2/5% CO_2. The submersion recording chamber was held at

34°C (TC-324B, Warner Instruments). Micropipettes were filled with (in mM): 135 potassium gluconate, 2 KCl, 4 NaCl, 10 Hepes, 0.2 EGTA, 4 ATP-Mg, 0.3 GTP-Tris, and 10 phosphocreatine-Tris (pH 7.25, 295 mOsm L^{-1}). 1 M KOH was used to adjust pH of the internal solution. Internal containing 1,2-bis(2-aminophenoxy)ethane-N,N,N', N'-tetraacetic acid (BAPTA) had concentrations of 10 µM. The approximate bath flowrate was 2 ml min^{-1} and the recording chamber held approximately 5 ml solution. The specific T-channel antagonist TTA-A2, generously provided by Dr Bruce Bean (Harvard University) or TTA-P2 (Alamone) were made into stock aliquots of 3 mM in DMSO; final concentration was 1 µM. 6-Cyano-7-nitroquinoxaline-2,3-dione (CNQX) at 2.5 µM was obtained from Sigma (St. Louis, MO, USA), and diluted into high-concentration stock solutions in DMSO or water before final dilution. Final DMSO concentration was always <0.2%.

The TRN was visualized under 5x magnification, and pairs of TRN cells were identified and patched under 40× IR-DIC optics (SliceScope, Scientifica, Uckfield, UK). Voltage signals were amplified and low-pass filtered at 8 kHz (MultiClamp, Axon Instruments, Molecular Devices, Sunnyvale, CA,USA), digitized at 20 kHz (custom Matlab routines controlling a National Instruments (Austin, TX, USA) USB6221 DAQ board), and data were stored for offline analysis in Matlab (Mathworks, R2017a, Natick, MA, USA). Recordings were made in whole-cell current-clamp mode. Values V_{rest} ranged from −50 to −70 mV. 500-ms pulses of negative injections of current were used to measure coupling, with amplitudes of injected current minimized in order to minimize T current activation in the injected cell, with a goal of 0.5 - 1 mV deflection in the coupled cell. Pipette resistances were 5-9 MΩ before bridge balance, which was removed if exceeding 25 MΩ. Voltages are reported uncorrected for the liquid junction potential.

Calcium imaging

To visualize calcium flux into and within coupled and uncoupled cells, 200 µM Oregon Green 488 BAPTA-1 (OGB-1) was added to the internal solution. An LED with wavelength 472 nm was delivered through the objective to excite the OGB-1. Images were captured at 30 fps through 40X IR-DIC optics (SliceScope, Scientifica, Uckfield, UK) and stored for offline analysis with Matlab. Regions of interest (ROIs) were chosen in the center of each recorded neuron, and changes in fluorescence normalized to baseline and background fluorescence were computed for each ROI.

Numerical Analysis

All numerical analysis was performed in Matlab (R2017). Input resistances (R_{in}) for each cell and coupling between cells were quantified by injecting 25-100 pA of hyperpolarizing current into one cell of a coupled pair and measuring the voltage deflection in that cell (ΔV) and in the couple neighbor (δV). Coupling coefficient (cc) is computed as δV/ΔV and are reported as averages of a set of 10 measurements, repeated every 2 min. Coupling conductances G_C were estimated separately for each direction (Fortier, 2010; Sevetson & Haas, 2015). Experiments were discarded if input resistance R_{in} of either cell deviated from its initial value by more than 20%. Changes in coupling were evaluated as the average over the first 20 minutes following activity, compared to the normalized baseline values, and are reported as means ± SEM. We report Student's *t*-tests as two-tailed paired comparisons of pre- and post-stimulus averages and report the results as p_t. Two-sided Wilcoxon signed rank tests were also carried out on the sets of change in coupling for each condition and are reported as p_s. No multiple comparisons were performed.

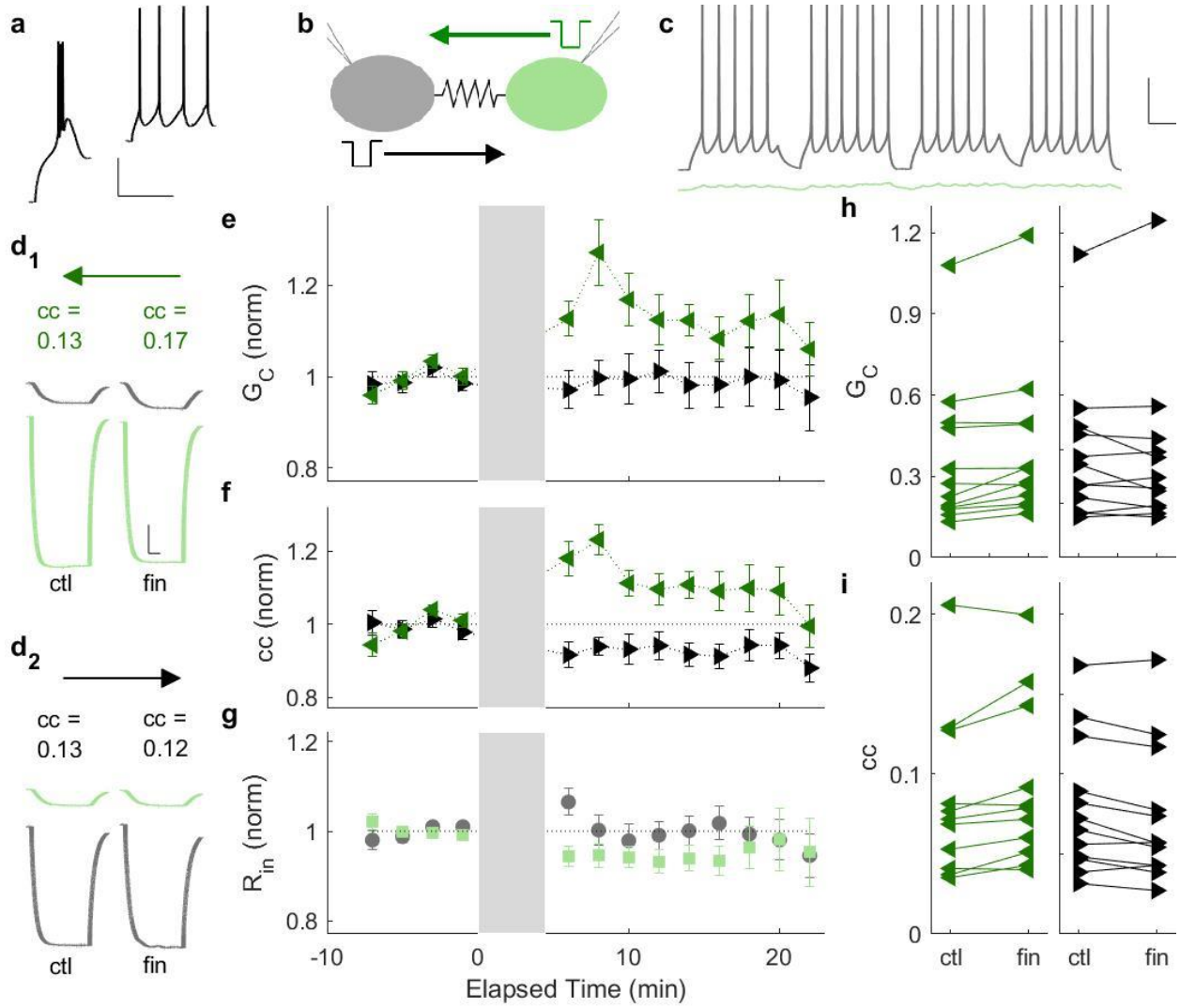

Figure 1. Long-term potentiation results from tonic firing in one cell of a coupled pair. A) TRN neurons fire bursts from hyperpolarized potentials (left; V_m = -82 mV) and tonic spikes from depolarized potentials (right; V_m = -55 mV). Scale bar 20 mV, 200 ms. B) Schematic of coupling measurement from an active cell (grey) and its electrically coupled neighbor (sage). C) Regular tonic spiking was driven by current injection into one cell (grey; V_m = -54 mV), while the coupled cell (sage) rests at -70 mV without stimulation. Experiments were performed with TTA in the bath. Scale bar 25 mV, 250 ms. D) Coupling coefficients (cc) for a pair before (left) and after (right) tonic spiking as shown in C. **cc** from the quiet cell into the active cell (green arrows) is

shown in the top panel, and **cc** in the reverse direction on bottom. E) Coupling conductance G_C shown for each direction, before and after stimulated spiking, normalized to pre-activity values (for G_C quiet→ active, ΔG_C = 15.5 ± 2.4%, p_t = 0.004; for G_C active→ quiet, ΔG_C = -1.5 ± 0.5%, p_t = 0.78; n = 12 pairs). F) **cc** for each direction (for quiet→ active, Δcc = 13.6 ± 2.2%, p_t = 0.01, n = 12; for active → quiet, Δcc = 7.6 ± 0.5%, p_t = 0.018; n = 12 pairs). G) Input resistance for both cells during the experiments. H) G_C for each pair used in D (for G_C quiet→ active, p_s = 0.0009; for active → quiet, p_s = 0.76). I) **cc** for each pair used in E (for cc quiet→ active, p_s = 0.01; for active → quiet, p_s = 0.019). p_t indicates 2-tailed, paired Student's t-test, and p_s is a Wilcoxon sign test.

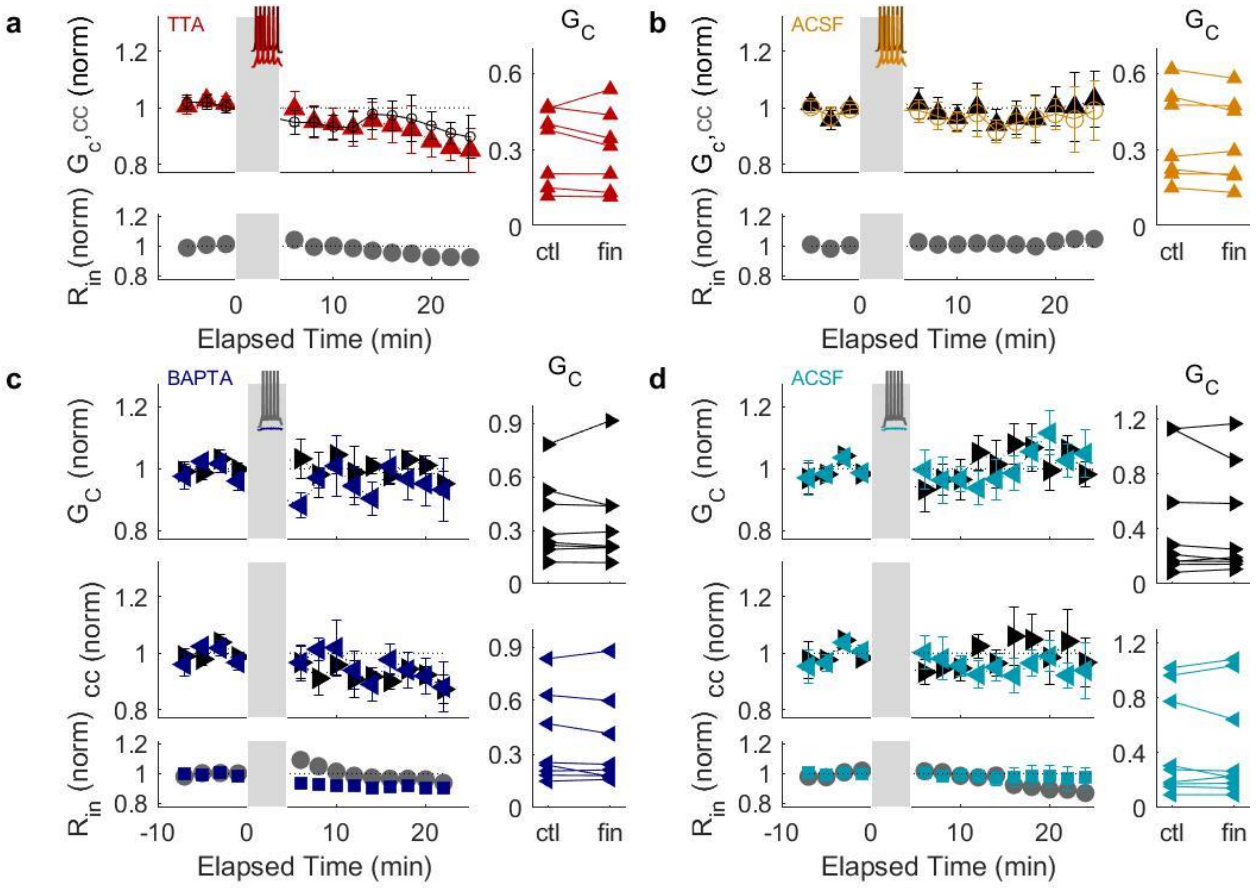

Figure 2. LTP is specific to single-cell stimulation and depends on calcium influx. A) cc and Gc before and after paired tonic spiking in TTA (averaged over both directions; for Δcc, p_t = 0.13, p_s = 0.12; for ΔG_C, p_t = 0.3, p_s = 0.2; n = 8 pairs). B) cc and Gc before and after paired tonic spiking in unmodified ACSF (averaged over both directions; for Δcc, p_t = 0.37, p_s = 0.46; for ΔG_C, p_t = 0.08, p_s = 0.07; n = 6 pairs). C) cc and Gc before and after single-cell spiking with calcium chelated by BAPTA in the internal. For ΔG_C active → quiet, p_t = 0.89, p_s = 0.84; for ΔG_C quiet → active, p_t = 0.34, p_s = 0.46; for Δcc active → quiet, p_t = 0.09, p_s = 0.07; for Δcc quiet → active, p_t = 0.66, p_s = 0.95 (n = 7 pairs). D) cc and Gc before and after single-cell tonic spiking in unmodified ACSF. For ΔG_C active → quiet, p_t = 0.38, p_s = 0.57; for ΔG_C quiet → active, p_t = 0.78, p_s = 0.82; for Δcc active → quiet, p_t = 0.4, p_s = 0.73; for Δcc quiet → active, p_t = 0.16, p_s = 0.25 (n = 9 pairs).

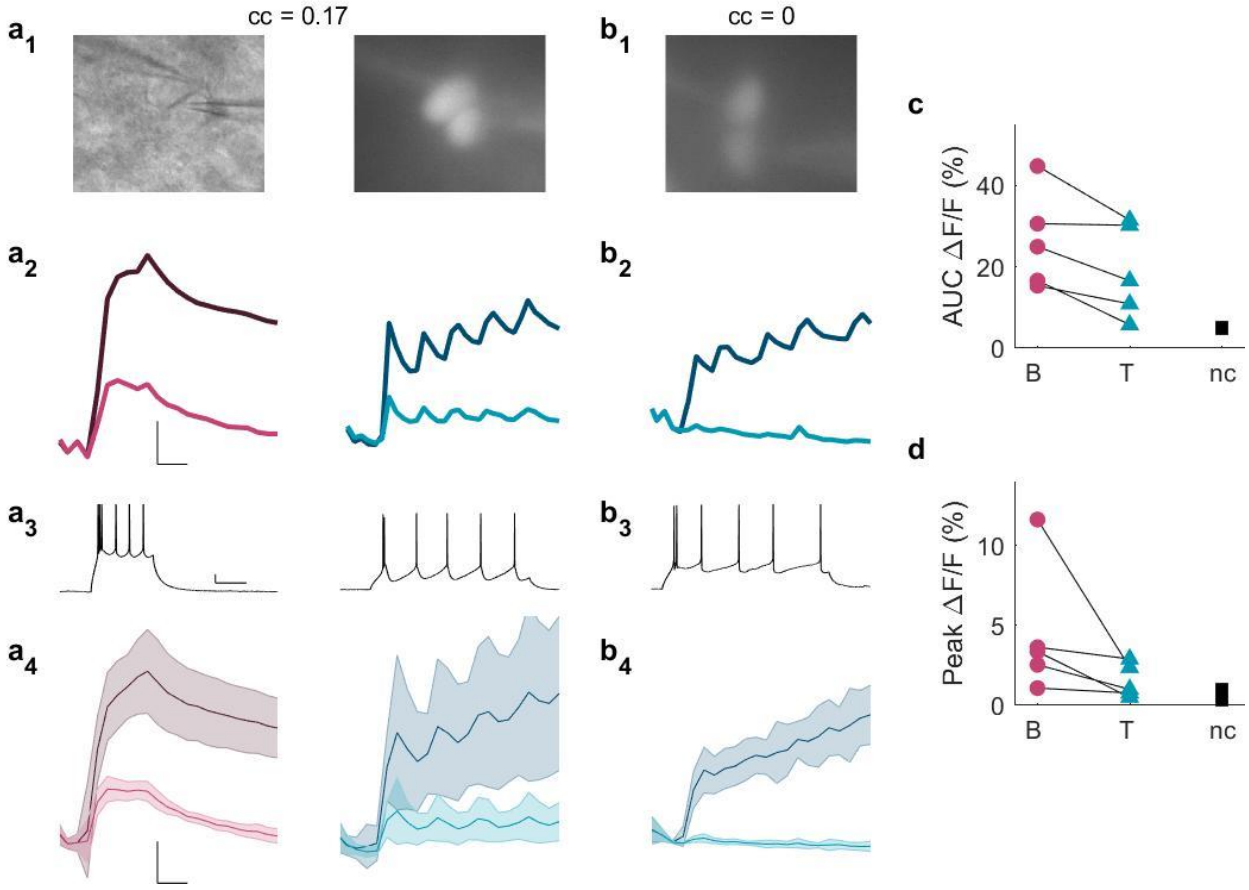

Figure 3. Calcium flows across the gap junction during spiking. A_1) IR-DIC and GFP images of a coupled pair (cc = 0.17). A_2) Calcium signals (ΔF/F) in a cell directly stimulated to burst (dark red) or spike tonically (dark blue), and calcium signals in the quiet cell (lighter shades) of a coupled pair. Scale bar 2.5%, 100 ms. A_3) Bursting (left) or tonic spikes (center) that drove responses in A_2. Scale bar 10 mV, 100 ms. A_4) Average calcium signals during bursting (reds) and tonic spiking (blues) in this coupled pair. B_1) GFP image of an uncoupled pair. Scale bar 2.5%, 100 ms. B_2) Calcium signals (ΔF/F) in a cell directly stimulated spike tonically (dark blue), and in the quiet uncoupled cell (light blue). B_3) Tonic spikes that drove responses in B_2. B_4) Average calcium signals during tonic spiking in uncoupled pairs (n = 2 pairs). C) Total (area under curve) ΔF/F in the quiet cell during bursting (B, red) and tonic spikes (T, blue) within each pair (mean difference -25.2 ± 10.6%, p_s = 0.06, n = 6 pairs), and for

335 uncoupled pairs (black, nc; n = 2 pairs). D) Peak ΔF/F in the quiet cell during bursting (B, red)

336 and tonic spikes (T, blue) within each pair (mean difference -56.6 ± 10.9%, p_s = 0.03, n = 6

337 pairs), and for uncoupled pairs (black, nc; n = 2 pairs).

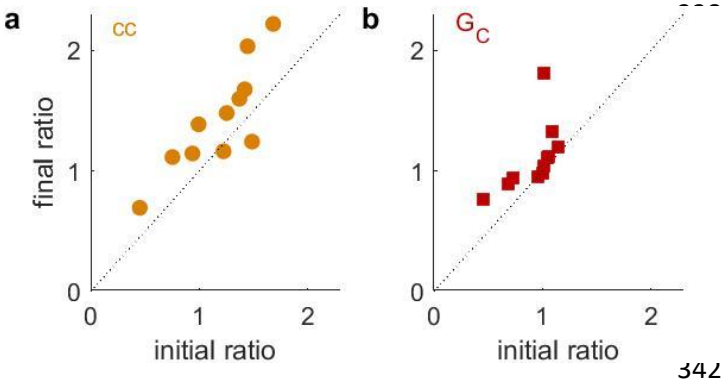

342

343 Figure 4. **LTP is expressed asymmetrically**. A) Asymmetry of coupling (**cc** into active cell / **cc**
344 from active cell) increased consistently across pairs following activity-induced LTP, plotted here
345 against initial values (mean change 24.3 ± 6.2%, p_t = 0.0015, p_s = 0.008, n = 12 pairs). B)
346 Asymmetry of coupling conductance (G_C into active cell / G_C from active cell) increased
347 consistently across pairs following activity-induced LTP, plotted against initial values (mean
348 change 22.4 ± 8.2%, p_t = 0.029, p_s = 0.008).

349

350

351

352

353

354

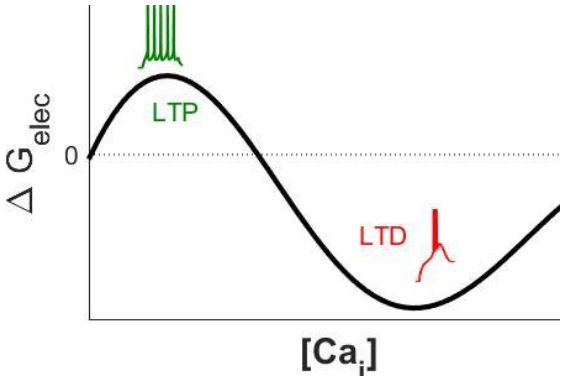

359 Figure 5. **Proposed calcium-based activity rule for electrical synapses**. Smaller influx of

360 calcium during tonic spiking (green) leads to LTP, while larger influx during bursting (red) leads

361 to LTD.

References

Apostolides, P. F., & Trussell, L. O. (2014). Control of Interneuron Firing by Subthreshold Synaptic Potentials in Principal Cells of the Dorsal Cochlear Nucleus. *Neuron*. Retrieved from http://www.ncbi.nlm.nih.gov/entrez/query.fcgi?cmd=Retrieve&db=PubMed&dopt=Citation&list_uids=25002229

Bennett, M. V., & Zukin, R. S. (2004). Electrical coupling and neuronal synchronization in the Mammalian brain. *Neuron, 41*(4), 495-511. Retrieved from http://www.ncbi.nlm.nih.gov/entrez/query.fcgi?cmd=Retrieve&db=PubMed&dopt=Citation&list_uids=14980200

Bienenstock, E. L., Cooper, L. N., & Munro, P. W. (1982). Theory for the development of neuron selectivity: orientation specificity and binocular interaction in visual cortex. *J Neurosci, 2*(1), 32-48. Retrieved from http://www.ncbi.nlm.nih.gov/entrez/query.fcgi?cmd=Retrieve&db=PubMed&dopt=Citation&list_uids=7054394

Budde, T., Munsch, T., & Pape, H. C. (1998). Distribution of L-type calcium channels in rat thalamic neurones. *Eur J Neurosci, 10*(2), 586-597. Retrieved from http://www.ncbi.nlm.nih.gov/pubmed/9749721

Chow, C. C., & Kopell, N. (2000). Dynamics of spiking neurons with electrical coupling. *Neural Comput, 12*(7), 1643-1678. Retrieved from http://www.ncbi.nlm.nih.gov/entrez/query.fcgi?cmd=Retrieve&db=PubMed&dopt=Citation&list_uids=10935921

Coesmans, M., Weber, J. T., De Zeeuw, C. I., & Hansel, C. (2004). Bidirectional parallel fiber plasticity in the cerebellum under climbing fiber control. *Neuron, 44*(4), 691-700. doi:10.1016/j.neuron.2004.10.031

Connors, B. W., & Long, M. A. (2004). Electrical synapses in the mammalian brain. *Annu Rev Neurosci, 27*, 393-418. Retrieved from http://www.ncbi.nlm.nih.gov/entrez/query.fcgi?cmd=Retrieve&db=PubMed&dopt=Citation&list_uids=15217338

Contreras, D., Curro Dossi, R., & Steriade, M. (1992). Bursting and tonic discharges in two classes of reticular thalamic neurons. *J Neurophysiol, 68*(3), 973-977. Retrieved from http://www.ncbi.nlm.nih.gov/entrez/query.fcgi?cmd=Retrieve&db=PubMed&dopt=Citation&list_uids=1432063

Coulon, P., & Landisman, C. E. (2017). The Potential Role of Gap Junctional Plasticity in the Regulation of State. *Neuron, 93*(6), 1275-1295. doi:10.1016/j.neuron.2017.02.041

Crunelli, V., Cope, D. W., & Hughes, S. W. (2006). Thalamic T-type Ca2+ channels and NREM sleep. *Cell Calcium, 40*(2), 175-190. doi:10.1016/j.ceca.2006.04.022

Destexhe, A. (1998). Spike-and-wave oscillations based on the properties of GABAB receptors. *J Neurosci, 18*(21), 9099-9111. Retrieved from http://www.ncbi.nlm.nih.gov/entrez/query.fcgi?cmd=Retrieve&db=PubMed&dopt=Citation&list_uids=9787013

Destexhe, A., Bal, T., McCormick, D. A., & Sejnowski, T. J. (1996). Ionic mechanisms underlying synchronized oscillations and propagating waves in a model of ferret thalamic slices. *J Neurophysiol, 76*(3), 2049-2070. Retrieved from http://www.ncbi.nlm.nih.gov/pubmed/8890314

Devor, A., & Yarom, Y. (2002). Electrotonic coupling in the inferior olivary nucleus revealed by simultaneous double patch recordings. *J Neurophysiol, 87*(6), 3048-3058. Retrieved from http://www.ncbi.nlm.nih.gov/entrez/query.fcgi?cmd=Retrieve&db=PubMed&dopt=Citation&list_uids=12037207

Draguhn, A., Traub, R. D., Schmitz, D., & Jefferys, J. G. (1998). Electrical coupling underlies high-frequency oscillations in the hippocampus in vitro. *Nature, 394*(6689), 189-192. Retrieved from http://www.ncbi.nlm.nih.gov/entrez/query.fcgi?cmd=Retrieve&db=PubMed&dopt=Citation&list_uids=9671303

Dudek, S. M., & Bear, M. F. (1992). Homosynaptic long-term depression in area CA1 of hippocampus and effects of N-methyl-D-aspartate receptor blockade. *Proc Natl Acad Sci U S A, 89*(10), 4363-4367. Retrieved from http://www.ncbi.nlm.nih.gov/entrez/query.fcgi?cmd=Retrieve&db=PubMed&dopt=Citation&list_uids=1350090

Ferrarelli, F., & Tononi, G. (2011). The thalamic reticular nucleus and schizophrenia. *Schizophr Bull, 37*(2), 306-315. Retrieved from http://www.ncbi.nlm.nih.gov/entrez/query.fcgi?cmd=Retrieve&db=PubMed&dopt=Citation&list_uids=21131368

Fortier, P. A. (2010). Detecting and estimating rectification of gap junction conductance based on simulations of dual-cell recordings from a pair and a network of coupled cells. *J Theor Biol, 265*(2), 104-114. Retrieved from http://www.ncbi.nlm.nih.gov/entrez/query.fcgi?cmd=Retrieve&db=PubMed&dopt=Citation&list_uids=20385146

Fuentealba, P., & Steriade, M. (2005). The reticular nucleus revisited: intrinsic and network properties of a thalamic pacemaker. *Progress in Neurobiology, 75*(2), 125-141. Retrieved from http://www.ncbi.nlm.nih.gov/entrez/query.fcgi?cmd=Retrieve&db=PubMed&dopt=Citation&list_uids=15784303

Galarreta, M., & Hestrin, S. (2001). Electrical synapses between GABA-releasing interneurons. *Nat Rev Neurosci, 2*(6), 425-433. Retrieved from http://www.ncbi.nlm.nih.gov/entrez/query.fcgi?cmd=Retrieve&db=PubMed&dopt=Citation&list_uids=11389476

Gutierrez, G. J., O'Leary, T., & Marder, E. (2013). Multiple mechanisms switch an electrically coupled, synaptically inhibited neuron between competing rhythmic oscillators. *Neuron, 77*(5), 845-858. doi:10.1016/j.neuron.2013.01.016

Haas, J. S. (2015). A new measure for the strength of electrical synapses. *Front Cell Neurosci, 9*, 378. Retrieved from http://www.ncbi.nlm.nih.gov/entrez/query.fcgi?cmd=Retrieve&db=PubMed&dopt=Citation&list_uids=26441546

Haas, J. S., & Landisman, C. E. (2012). State-dependent modulation of gap junction signaling by the persistent sodium current. *Front Cell Neurosci, 5*, 31. Retrieved from http://www.ncbi.nlm.nih.gov/entrez/query.fcgi?cmd=Retrieve&db=PubMed&dopt=Citation&list_uids=22319469

Haas, J. S., Zavala, B., & Landisman, C. E. (2011). Activity-dependent long-term depression of electrical synapses. *Science, 334*(6054), 389-393. Retrieved from http://www.ncbi.nlm.nih.gov/entrez/query.fcgi?cmd=Retrieve&db=PubMed&dopt=Citation&list_uids=22021860

Halassa, M. M., Chen, Z., Wimmer, R. D., Brunetti, P. M., Zhao, S., Zikopoulos, B., . . . Wilson, M. A. (2014). State-dependent architecture of thalamic reticular subnetworks. *Cell, 158*(4), 808-821. Retrieved from

http://www.ncbi.nlm.nih.gov/entrez/query.fcgi?cmd=Retrieve&db=PubMed&dopt=Citation&list_uids=25126786

Hou, G., Smith, A. G., & Zhang, Z. W. (2016). Lack of Intrinsic GABAergic Connections in the Thalamic Reticular Nucleus of the Mouse. *J Neurosci, 36*(27), 7246-7252. doi:10.1523/JNEUROSCI.0607-16.2016

Huguenard, J. R., & Prince, D. A. (1992). A novel T-type current underlies prolonged Ca(2+)-dependent burst firing in GABAergic neurons of rat thalamic reticular nucleus. *J Neurosci, 12*(10), 3804-3817. Retrieved from http://www.ncbi.nlm.nih.gov/entrez/query.fcgi?cmd=Retrieve&db=PubMed&dopt=Citation&list_uids=1403085

Kimura, A. (2014). Diverse subthreshold cross-modal sensory interactions in the thalamic reticular nucleus: implications for new pathways of cross-modal attentional gating function. *Eur J Neurosci, 39*(9), 1405-1418. Retrieved from http://www.ncbi.nlm.nih.gov/entrez/query.fcgi?cmd=Retrieve&db=PubMed&dopt=Citation&list_uids=24646412

Kothmann, W. W., Li, X., Burr, G. S., & O'Brien, J. (2007). Connexin 35/36 is phosphorylated at regulatory sites in the retina. *Vis Neurosci, 24*(3), 363-375. doi:10.1017/S095252380707037X

Kraus, R. L., Li, Y., Gregan, Y., Gotter, A. L., Uebele, V. N., Fox, S. V., . . . Renger, J. J. (2010). In vitro characterization of T-type calcium channel antagonist TTA-A2 and in vivo effects on arousal in mice. *J Pharmacol Exp Ther, 335*(2), 409-417. doi:10.1124/jpet.110.171058

Landisman, C. E., & Connors, B. W. (2005). Long-term modulation of electrical synapses in the mammalian thalamus. *Science, 310*(5755), 1809-1813. Retrieved from http://www.ncbi.nlm.nih.gov/entrez/query.fcgi?cmd=Retrieve&db=PubMed&dopt=Citation&list_uids=16357260

Landisman, C. E., Long, M. A., Beierlein, M., Deans, M. R., Paul, D. L., & Connors, B. W. (2002). Electrical synapses in the thalamic reticular nucleus. *J Neurosci, 22*(3), 1002-1009. Retrieved from http://www.ncbi.nlm.nih.gov/entrez/query.fcgi?cmd=Retrieve&db=PubMed&dopt=Citation&list_uids=11826128

Lefler, Y., Yarom, Y., & Uusisaari, M. Y. (2014). Cerebellar inhibitory input to the inferior olive decreases electrical coupling and blocks subthreshold oscillations. *Neuron, 81*(6), 1389-1400. Retrieved from http://www.ncbi.nlm.nih.gov/entrez/query.fcgi?cmd=Retrieve&db=PubMed&dopt=Citation&list_uids=24656256

Lisman, J. (1989). A mechanism for the Hebb and the anti-Hebb processes underlying learning and memory. *Proc Natl Acad Sci U S A, 86*(23), 9574-9578. Retrieved from http://www.ncbi.nlm.nih.gov/pubmed/2556718

Lisman, J. E. (2001). Three Ca2+ levels affect plasticity differently: the LTP zone, the LTD zone and no man's land. *J Physiol, 532*(Pt 2), 285. Retrieved from http://www.ncbi.nlm.nih.gov/pubmed/11306649

Lynn, B. D., Li, X., Hormuzdi, S. G., Griffiths, E. K., McGlade, C. J., & Nagy, J. I. (2018). E3 ubiquitin ligases LNX1 and LNX2 localize at neuronal gap junctions formed by connexin36 in rodent brain and molecularly interact with connexin36. *Eur J Neurosci*. doi:10.1111/ejn.14198

Malenka, R. C., & Bear, M. F. (2004). LTP and LTD: an embarrassment of riches. *Neuron, 44*(1), 5-21. Retrieved from http://www.ncbi.nlm.nih.gov/entrez/query.fcgi?cmd=Retrieve&db=PubMed&dopt=Citation&list_uids=15450156

Malenka, R. C., Kauer, J. A., Perkel, D. J., & Nicoll, R. A. (1989). The impact of postsynaptic calcium on synaptic transmission--its role in long-term potentiation. *Trends Neurosci, 12*(11), 444-450.

503 Retrieved from
504 http://www.ncbi.nlm.nih.gov/entrez/query.fcgi?cmd=Retrieve&db=PubMed&dopt=Citation&list
505 _uids=2479146
506 Marsh, A. J., Michel, J. C., Adke, A. P., Heckman, E. L., & Miller, A. C. (2017). Asymmetry of an
507 Intracellular Scaffold at Vertebrate Electrical Synapses. *Curr Biol, 27*(22), 3561-3567 e3564.
508 doi:10.1016/j.cub.2017.10.011
509 Mathy, A., Clark, B. A., & Hausser, M. (2014). Synaptically induced long-term modulation of electrical
510 coupling in the inferior olive. *Neuron, 81*(6), 1290-1296. Retrieved from
511 http://www.ncbi.nlm.nih.gov/entrez/query.fcgi?cmd=Retrieve&db=PubMed&dopt=Citation&list
512 _uids=24656251
513 McAlonan, K., Cavanaugh, J., & Wurtz, R. H. (2006). Attentional modulation of thalamic reticular
514 neurons. *J Neurosci, 26*(16), 4444-4450. Retrieved from
515 http://www.ncbi.nlm.nih.gov/entrez/query.fcgi?cmd=Retrieve&db=PubMed&dopt=Citation&list
516 _uids=16624964
517 McCormick, D. A., & Bal, T. (1997). Sleep and arousal: thalamocortical mechanisms. *Annu Rev Neurosci,*
518 *20*, 185-215. doi:10.1146/annurev.neuro.20.1.185
519 McMahon, D. G., Knapp, A. G., & Dowling, J. E. (1989). Horizontal cell gap junctions: single-channel
520 conductance and modulation by dopamine. *Proc Natl Acad Sci U S A, 86*(19), 7639-7643.
521 Retrieved from
522 http://www.ncbi.nlm.nih.gov/entrez/query.fcgi?cmd=Retrieve&db=PubMed&dopt=Citation&list
523 _uids=2477845
524 Otsuka, T., & Kawaguchi, Y. (2013). Common excitatory synaptic inputs to electrically connected cortical
525 fast-spiking cell networks. *J Neurophysiol, 110*(4), 795-806. doi:10.1152/jn.00071.2013
526 Pereda, A. E., & Faber, D. S. (1996). Activity-dependent short-term enhancement of intercellular
527 coupling. *J Neurosci, 16*(3), 983-992. Retrieved from
528 http://www.ncbi.nlm.nih.gov/entrez/query.fcgi?cmd=Retrieve&db=PubMed&dopt=Citation&list
529 _uids=8558267
530 Pernelle, G., Nicola, W., & Clopath, C. (2018). Gap junction plasticity as a mechanism to regulate
531 network-wide oscillations. *PLoS Comput Biol, 14*(3), e1006025.
532 doi:10.1371/journal.pcbi.1006025
533 Pfeuty, B., Mato, G., Golomb, D., & Hansel, D. (2005). The combined effects of inhibitory and electrical
534 synapses in synchrony. *Neural Comput, 17*(3), 633-670. Retrieved from
535 http://www.ncbi.nlm.nih.gov/entrez/query.fcgi?cmd=Retrieve&db=PubMed&dopt=Citation&list
536 _uids=15802009
537 Pham, T., & Haas, J. S. (2018). Electrical synapses between inhibitory neurons shape the responses of
538 principal neurons to transient inputs in the thalamus: a modeling study. *Sci Rep, 8*(1), 7763.
539 doi:10.1038/s41598-018-25956-x
540 Pham, T., & Haas, J. S. (2019). Electrical synapses regulate both subthreshold integration and population
541 activity of principal cells in response to transient inputs within canonical feedforward circuits.
542 *PLoS Comput Biol, 15*(2), e1006440. doi:10.1371/journal.pcbi.1006440
543 Pinault, D. (2004). The thalamic reticular nucleus: structure, function and concept. *Brain Res Brain Res*
544 *Rev, 46*(1), 1-31. doi:10.1016/j.brainresrev.2004.04.008
545 Sevetson, J., Fittro, S., Heckman, E., & Haas, J. S. (2017). A calcium-dependent pathway underlies
546 activity-dependent plasticity of electrical synapses in the thalamic reticular nucleus. *J Physiol,*
547 *595*(13), 4417-4430. doi:10.1113/JP274049
548 Sevetson, J., & Haas, J. S. (2015). Asymmetry and modulation of spike timing in electrically coupled
549 neurons. *J Neurophysiol*, jn 00843 02014. Retrieved from

http://www.ncbi.nlm.nih.gov/entrez/query.fcgi?cmd=Retrieve&db=PubMed&dopt=Citation&list_uids=25540226

Sherman, S. M. (2016). Thalamus plays a central role in ongoing cortical functioning. *Nat Neurosci, 19*(4), 533-541. doi:10.1038/nn.4269

Snipas, M., Rimkute, L., Kraujalis, T., Maciunas, K., & Bukauskas, F. F. (2017). Functional asymmetry and plasticity of electrical synapses interconnecting neurons through a 36-state model of gap junction channel gating. *PLoS Comput Biol, 13*(4), e1005464. doi:10.1371/journal.pcbi.1005464

Sorokin, J. M., Davidson, T. J., Frechette, E., Abramian, A. M., Deisseroth, K., Huguenard, J. R., & Paz, J. T. (2017). Bidirectional Control of Generalized Epilepsy Networks via Rapid Real-Time Switching of Firing Mode. *Neuron, 93*(1), 194-210. doi:10.1016/j.neuron.2016.11.026

Soto-Sanchez, C., Wang, X., Vaingankar, V., Sommer, F. T., & Hirsch, J. A. (2017). Spatial scale of receptive fields in the visual sector of the cat thalamic reticular nucleus. *Nat Commun, 8*(1), 800. doi:10.1038/s41467-017-00762-7

Srinivas, M., Rozental, R., Kojima, T., Dermietzel, R., Mehler, M., Condorelli, D. F., . . . Spray, D. C. (1999). Functional properties of channels formed by the neuronal gap junction protein connexin36. *J Neurosci, 19*(22), 9848-9855. Retrieved from http://www.ncbi.nlm.nih.gov/entrez/query.fcgi?cmd=Retrieve&db=PubMed&dopt=Citation&list_uids=10559394

Steriade, M., McCormick, D. A., & Sejnowski, T. J. (1993). Thalamocortical oscillations in the sleeping and aroused brain. *Science, 262*(5134), 679-685. Retrieved from http://www.ncbi.nlm.nih.gov/entrez/query.fcgi?cmd=Retrieve&db=PubMed&dopt=Citation&list_uids=8235588

Turecek, J., Yuen, G. S., Han, V. Z., Zeng, X. H., Bayer, K. U., & Welsh, J. P. (2014). NMDA receptor activation strengthens weak electrical coupling in mammalian brain. *Neuron, 81*(6), 1375-1388. Retrieved from http://www.ncbi.nlm.nih.gov/entrez/query.fcgi?cmd=Retrieve&db=PubMed&dopt=Citation&list_uids=24656255

Vervaeke, K., Lorincz, A., Gleeson, P., Farinella, M., Nusser, Z., & Silver, R. A. (2010). Rapid desynchronization of an electrically coupled interneuron network with sparse excitatory synaptic input. *Neuron, 67*(3), 435-451. Retrieved from http://www.ncbi.nlm.nih.gov/entrez/query.fcgi?cmd=Retrieve&db=PubMed&dopt=Citation&list_uids=20696381

Wang, X. J., & Rinzel, J. (1993). Spindle rhythmicity in the reticularis thalami nucleus: synchronization among mutually inhibitory neurons. *Neuroscience, 53*(4), 899-904. Retrieved from http://www.ncbi.nlm.nih.gov/entrez/query.fcgi?cmd=Retrieve&db=PubMed&dopt=Citation&list_uids=8389430

Welzel, G., & Schuster, S. (2018). Long-term potentiation in an innexin-based electrical synapse. *Scientific Reports, 8*. doi:ARTN 12579

10.1038/s41598-018-30966-w

Whittington, M. A., & Traub, R. D. (2003). Interneuron diversity series: inhibitory interneurons and network oscillations in vitro. *Trends Neurosci, 26*(12), 676-682. Retrieved from http://www.ncbi.nlm.nih.gov/entrez/query.fcgi?cmd=Retrieve&db=PubMed&dopt=Citation&list_uids=14624852

Yang, X. D., Korn, H., & Faber, D. S. (1990). Long-term potentiation of electrotonic coupling at mixed synapses. *Nature, 348*(6301), 542-545. Retrieved from http://www.ncbi.nlm.nih.gov/entrez/query.fcgi?cmd=Retrieve&db=PubMed&dopt=Citation&list_uids=2174130

Yao, X., Cafaro, J., McLaughlin, A. J., Postma, F. R., Paul, D. L., Awatramani, G., & Field, G. D. (2018). Gap Junctions Contribute to Differential Light Adaptation across Direction-Selective Retinal Ganglion Cells. *Neuron, 100*(1), 216-228 e216. doi:10.1016/j.neuron.2018.08.021

Zikopoulos, B., & Barbas, H. (2012). Pathways for emotions and attention converge on the thalamic reticular nucleus in primates. *J Neurosci, 32*(15), 5338-5350. Retrieved from http://www.ncbi.nlm.nih.gov/entrez/query.fcgi?cmd=Retrieve&db=PubMed&dopt=Citation&list_uids=22496579

Zolnik, T. A., & Connors, B. W. (2016). Electrical synapses and the development of inhibitory circuits in the thalamus. *J Physiol, 594*(10), 2579-2592. doi:10.1113/JP271880